Electronic properties and dopant pairing behavior of manganese in boron-doped silicon

T. Roth,[a] P. Rosenits, S. Diez,[b] and S. W. Glunz
Fraunhofer Institute for Solar Energy Systems (ISE), Heidenhofstrasse 2, 79110 Freiburg, Germany

D. Macdonald
Department of Engineering, College of Engineering and Computer Science, The Australian National University, Canberra ACT 0200, Australia

S. Beljakowa and G. Pensl
Lehrstuhl für Angewandte Physik (LAP), University of Erlangen Nürnberg, 91058 Erlangen, Germany

(Received 30 May 2007; accepted 23 September 2007; published online 28 November 2007)

Boron-doped silicon wafers implanted with low doses of manganese have been analyzed by means of deep-level transient spectroscopy (DLTS), injection-dependent lifetime spectroscopy, and temperature-dependent lifetime spectroscopy. While DLTS measurements allow the defect levels and majority carrier capture cross sections to be determined, the lifetime spectroscopy techniques allow analysis of the dominant recombination levels and the corresponding ratios of the capture cross sections. Interstitial manganese and manganese-boron pairs were found to coexist, and their defect parameters have been investigated. In good agreement with the literature, this study identifies the defect level of manganese-boron pairs to be located in the lower half of the band gap at an energy level of $E_v+0.55$ eV with a majority carrier capture cross section of $\sigma_p=3.5\times10^{-13}$ cm^2. The capture cross-section ratio was found to be $k=\sigma_n/\sigma_p=6.0$. This implies that the previously unknown minority carrier capture cross section is $\sigma_n=2.1\times10^{12}$ cm^2. Concerning the defect related to interstitial manganese, this study identifies the most recombination-active level to be located in the upper half of the band gap at $E_C-0.45$ eV with a corresponding ratio of the capture cross sections of $k=9.4$. In addition, the temperature-dependent association time constant of manganese-boron pairs is determined to be $\tau_{\mathrm{assoc,Mn}}=8.3\times10^5$ K^{-1} cm^{-3} (T/N_{dop}) $\exp(0.67\ \mathrm{eV}/k_BT)$ and found to differ from that for iron by a factor of 3 at room temperature, allowing this association time constant to be used as a fingerprint for a possible contamination with manganese. Also, the diffusion coefficient of interstitial manganese in silicon is determined from these experiments in a temperature range from 70 to 120 °C. It can be represented by the expression $D_{\mathrm{Mn}}=6.9\times10^{-4}$ cm^2 s^{-1} $\exp(-0.67\ \mathrm{eV}/k_BT)$. © *2007 American Institute of Physics*.
[DOI: 10.1063/1.2812698]

I. INTRODUCTION

In the past decades, great efforts have been expended to identify and analyze the electrical properties of 3*d* transition-metal impurities in silicon. Knowledge of the energy levels within the band gap, the capture cross sections, as well as a proper understanding of any pairing behavior with other impurities or dopants is of both theoretical and technological interest. Due to the strong influence of material quality on the efficiency of solar cells, analyzing recombination-active defects introduced during crystal growth and solar cell processing is an especially important task in the field of silicon photovoltaics.

Manganese is located in the middle of the 3*d* transition metals between the light and slowly diffusing metals such as titanium and vanadium and the heavy and fast-diffusing metals such as nickel and copper, exhibiting a very similar diffusivity and solubility to iron. This makes it potentially dangerous, since it may introduce point-like defects into the silicon bulk at relatively high concentrations, resulting in considerable negative effects for devices such as solar cells.

Despite this ability to reduce the electrical quality of the silicon material, there have been few publications so far dealing with the analysis of manganese-related defects in silicon. The intention of this paper is to reveal the impact of manganese impurities on the electrical properties by analyzing the relevant defect parameters by means of deep-level transient spectroscopy (DLTS) and lifetime spectroscopy (LS). LS techniques have been shown to be an ideal complement to the well-established DLTS measurements when analyzing recombination-active defects in silicon.[1] In addition, by using dynamic lifetime measurements, the association behavior of manganese-boron pairs and the diffusivity of manganese in silicon will be investigated in detail.

II. ELECTRICAL PROPERTIES OF MANGANESE IN SILICON

Manganese forms part of the 3*d* transition metals and is located between chromium and iron in the Periodic Table. The only naturally occurring isotope is $^{55}_{25}$Mn with an atomic

[a]Electronic mail: thomas.roth@ise.fraunhofer.de
[b]Present address: Q-Cells AG, Thalheim, Germany.

TABLE I. Reported energy levels for interstitial manganese (Mn_i). The values summarized by Graff are average values from various DLTS measurements, while in this work temperature-dependent lifetime spectroscopy has been used.

Investigated defect: Interstitial manganese (Mn_i) in silicon	
Reference	Defect energy level E_t (eV)
Graff[2]	$E_C-0.12$
	$E_C-0.43$
	$E_V+0.27$
This work	$E_C-0.45$
	(0.405–0.495)

mass of $m_a=54.94u$ ($u=1.6605\times10^{-27}$ kg) and a nuclear charge of $25q$, with $q=1.6022\times10^{-19}$ C signifying the elementary charge. The solubility and diffusivity of manganese atoms within the silicon crystal lattice are relatively high and quite similar to iron[2] in the temperature range of 300–1500 K.

If impurity atoms are introduced into the silicon crystal, they can in general take up interstitial or substitutional places, as well as forming pairs, clusters, or precipitates with each other or different atoms that are present in the crystal. It was discovered very early that manganese exists in silicon in a stable interstitial form (Mn_i) as well as substitutionally (Mn_s).[3,4] In addition, it is known that manganese forms donor-acceptor pairs with boron, aluminum, gallium, tin, and gold.[2] Pairing with further metals has not been observed yet, but cannot be excluded either. A particularity of manganese is the formation of Mn_4 clusters consisting of four interstitial Mn atoms.[2]

The structure, charge states, and energy levels of Mn-related centers in silicon have been investigated in several studies since the 1950s. The energy levels and majority capture cross sections of interstitial manganese are quite well-established, with the most significant studies summarized by Graff,[2] who presents a weighted average for the defect parameters (see Table I). Mn_i occurs in four different charge states, leading to three energy levels in the band gap: an acceptor at $E_C-0.12$ eV, a donor at $E_C-0.43$ eV, and a double donor at $E_v+0.27$ eV.

For the second defect configuration of manganese, namely the manganese-boron pairs, publications concerning its defect parameters are less numerous[5–8] and listed in Table II. These investigations concluded that MnB pairs introduce one single deep donor level in the silicon band gap, with reported values ranging from $E_C-0.50$ to $E_C-0.57$ eV.

TABLE II. Reported energy levels for manganese-boron (MnB) pairs. The data have been evaluated mainly by means of deep-level transient spectroscopy (DLTS). The value determined in this work is the mean value of the DLTS measurements on two samples, while the error was calculated using weighted average calculations.

Investigated defect: Manganese-boron (MnB) pairs in silicon	
Reference	Defect energy level E_t (eV)
Carlson[5]	$E_C-0.53$
Lemke[7]	$E_C-0.55$
Lemke[8]	$E_C-0.57$
Nakashima *et al.*[6]	$E_C-0.50$
This work	$(E_V+0.55)\pm0.02$

Finally, there are a few quantitative studies about the defect parameters of substitutional manganese in silicon,[6,9–11] indicating that Mn_s exists in three charge states, leading to an acceptor level in the upper-band-gap half and a donor level in the lower-band-gap half.

In summary, it can be said that manganese shows a far more complex defect structure than iron or chromium for instance, which do not normally exist in substitutional form and also only exhibit one single interstitial energy level in the silicon band gap. A consequence of these additional energy levels for Mn is that it is difficult to state *a priori* which level dominates recombination, as the populations of the various charge states will depend on the Fermi level, i.e., on doping type and concentration. Under strong charge-carrier injection, the quasi-Fermi-levels influence the occupation of the different charge states as well, which means that the dominant recombination level can, in principle, also change depending on the injection density.

III. SAMPLE PREPARATION

The silicon wafers used in this study were float-zone grown with a surface orientation of ⟨100⟩. The samples were boron-doped with resistivities of either 1 Ω cm ($N_A=1.5\times10^{16}$ cm^{-3}, 460 μm thick), 20 Ω cm ($N_A=6.8\times10^{14}$ cm^{-3}, 500 μm thick), or 40 Ω cm ($N_A=3.4\times10^{14}$ cm^{-3}, 200 μm thick).

Prior to Mn implantation, the wafers were etched in a HF/HNO_3 solution to remove surface damage, and then RCA cleaned. Samples of each resistivity were then implanted with MnO^- ions at an energy of 70 keV to a dose of 5×10^{11} cm^{-2} on one side only. The MnO^- ions were extracted using a Cs ion source from a Cu cathode housing containing a pressed mixture of MnO_2 and Ag powders (approximately 8:1 by volume). The implantations were performed through a silicon aperture with dimensions of 30×30 mm^2, giving an implanted region of a sufficiently large area for subsequent measurements.

Following further surface cleaning and native oxide removal, the samples were annealed in a clean quartz-tube furnace in N_2 gas at 900 °C for 100 min to distribute the implanted Mn throughout the samples, followed by rapid cooling in air to room temperature. Interstitial Mn has a diffusivity of approximately 1.5×10^{-6} cm^2 s^{-1} at 900 °C,[2] resulting in a diffusion length of 930 μm for these annealing conditions, significantly greater than the wafer thickness. In the absence of precipitation, this should result in an approximately uniform distribution of Mn throughout the thickness of the wafers, with equivalent volume concentrations of approximately 1.0×10^{13} cm^{-3} for the 1 Ω cm and the 20 Ω cm samples and 2.5×10^{13} cm^{-3} for the 40 Ω cm sample, respectively. Note that the solid solubility limit of interstitial Mn at 900 °C is approximately 6×10^{13} cm^{-3}.[2] This is above the targeted volume concentrations, meaning that precipitation should indeed be avoided.

Note also that any lifetime-reducing crystal damage caused by the low doses and energy used here have previ-

ously been shown to be effectively removed during such annealing.[12] This allows us to attribute any reduction in carrier lifetime after annealing to the presence of the implanted atoms themselves. Although at 900 °C the majority of the Mn is likely to be in interstitial form, it is possible that during cooling some of this Mn moves to substitutional sites, as some studies indicate that substitutional Mn has a higher solubility at temperatures near 700 °C.[13]

Following annealing, the samples were again etched and cleaned, and then received 70-nm-thick plasma-enhanced chemical vapor deposited (PECVD) silicon nitride films on each surface. These films passivate the surfaces for sensitive measurement of the bulk lifetime.

It was necessary to implant MnO^- ions due to the very low yield of Mn ions. It is assumed that the MnO molecules break up upon implantation. This results in separated Mn and O atoms in the thin implanted subsurface region, which are then distributed throughout the wafer thickness by the annealing. Considering that the average O concentration after annealing corresponding to the doses used here is much less than the natural oxygen concentration in this material, the implanted O atoms are not expected to significantly affect the subsequent lifetime measurements. In recent publications,[14,15] it was indeed shown that the coimplantation of O had no serious effect on the measured bulk lifetime for the *p*-type samples analyzed here.

In addition, control samples that received no implantation were coprocessed. These allow the effect of other recombination channels, such as imperfect surface passivation, furnace contamination, and native defects or impurities in the starting material, to be assessed.

IV. EXPERIMENTAL TECHNIQUES

In order to extract the defect parameters of the different defect levels that manganese (Mn) can introduce into silicon (Si), various measurement techniques were used that turned out to complement each other very well.

The central concept of deep-level transient spectroscopy (DLTS)[16] is to fill the impurity traps with charge carriers and monitor their subsequent thermal emission into the majority carrier band. Performing DLTS scan transients at different temperatures, the energy levels and related majority carrier capture cross sections can be extracted. With the standard filling pulse technique, DLTS can only monitor deep defect centers in the band-gap half related to the majority charge carriers.

For the lifetime measurements, two recent but now well-established contactless techniques have been applied.[17] Injection-dependent lifetime spectroscopy (IDLS) curves were measured by means of the quasi-steady-state photoconductance technique (QSSPC) using the WCT-100 apparatus.[18] With this device, the effective minority carrier lifetime can be measured at a temperature of $T=(304\pm3)$ K as a function of the excess carrier concentration. On the other hand, temperature-dependent lifetime spectroscopy (TDLS) is based on the determination of the effective lifetime under low-level injection. We measured the TDLS curves by means of the microwave-detected photoconductance decay technique (MW-PCD)[19–21] using an integrated liquid-nitrogen-cooled cryostat. To best approach low-level injection conditions in the whole temperature range of the TDLS curve, the lifetime measurements have been performed at the minimum bias light intensity required to exclude distortions of the monoexponential photoconductance decay due to trapping effects.[17]

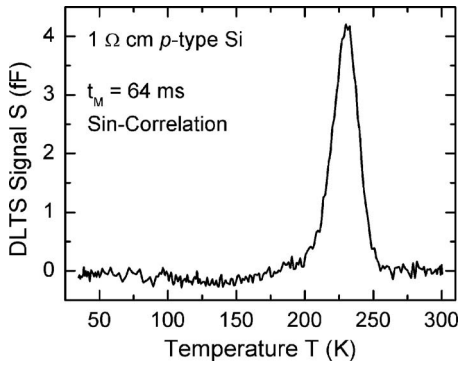

FIG. 1. DLTS spectrum of the Mn-contaminated 1 Ω cm sample for a sine correlation function.

V. EXPERIMENTAL RESULTS

A. Deep-level transient spectroscopy (DLTS)

After initial lifetime measurements and analysis,[14,15] a selection of the intentionally Mn-contaminated samples were prepared for DLTS measurements. This requires a Schottky contact on one side and an Ohmic contact on the other side of the sample. After standard HF etching, the contacts were sputtered onto the silicon wafers in a sputtering chamber at 2×10^{-6} mbar and at temperatures not above 55 °C. To achieve a Schottky contact on *p*-type material, 30 nm of titanium and 60 nm of aluminum were evaporated on one side of the samples through a mask allowing distinct circular contact areas with diameters of 0.20, 0.35, 0.60, and 1.00 mm. The Ohmic contact on the other side was achieved by covering the back side of the wafer entirely with a 60-nm aluminum layer.

The DLTS measurements were carried out using a digital DLTS system FT1030 from PhysTech. Fourier-based weighting functions were used to calculate the DLTS spectrum from the measured capacitance transients.

In Fig. 1, a DLTS spectrum taken on the Mn-contaminated 1 Ω cm sample for the sin correlation function is plotted, showing a satisfactory signal-to-noise ratio. Note that any additional contamination with iron during sample preparation would have led to a DLTS peak around 50 K, being related to iron-boron pairs with an energy level of $E_V+0.10$ eV.[22] However, only one peak was observed at around 225 K. In Fig. 2, the resulting Arrhenius plot based on the different correlation functions is shown. From the slope, an energy level of $E_t-E_V=0.56\pm0.03$ eV and a majority carrier capture cross section of $\sigma_p=5.2\times10^{-13}$ cm^2 are extracted. Please note that the indicated uncertainty includes systematic uncertainties due to the experimental DLTS setup. The defect density of $N_t=3.5\times10^{13}$ cm^{-3} is obtained from the DLTS peak height. As usual for DLTS

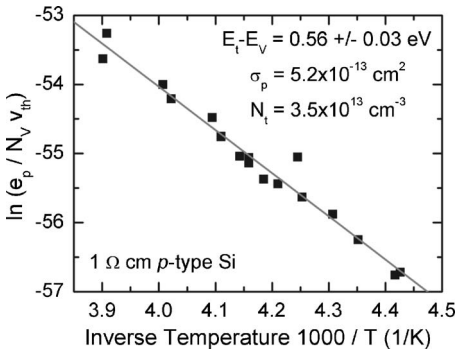

FIG. 2. Arrhenius plot of the DLTS data for the 1 Ω cm sample. In the inset. the extracted defect parameters are shown.

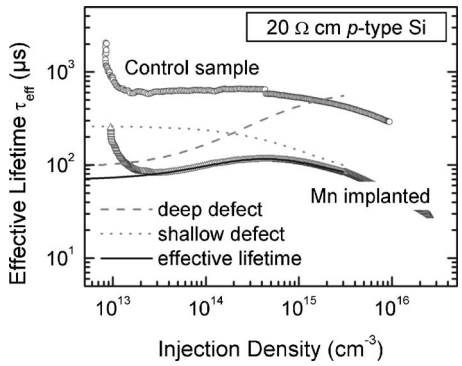

FIG. 3. Injection-dependent lifetime of a control sample and the Mn implanted 20 Ω cm sample. The lifetime of the control sample is about one order of magnitude higher than the lifetime of the implanted sample, showing that surface passivation is sufficient. The abnormally high lifetime below an injection density of 3×10^{13} cm^{-3} is caused by measurement artifacts, and does not reflect the true recombination lifetime. The data for the Mn-implanted sample in an injection density range of 3×10^{13} to 3×10^{15} cm^{-3} has been modeled with SRH theory including a deep (dashed line) and a shallow (dotted line) defect level, allowing a very good fit.

measurements, the value of the capture cross section has to be treated with caution, since this value is obtained from the extrapolation of the Arrhenius fit to infinite temperatures on a logarithmic scale.

A similar DLTS analysis was performed for the Mn-contaminated sample having a resistivity of 40 Ω cm, yielding an energy level of $E_t-E_v=0.53\pm0.03$ eV, a majority carrier capture cross section of $\sigma_p=1.8\times10^{-13}$ cm^2, and a defect density of $N_t=8.2\times10^{11}$ cm^{-3}. This measured defect concentration is more than one order of magnitude lower than the expected concentration from the implanted dose. It is not known if this was caused by a problem during the implantation, precipitation during annealing, or during DLTS measurements. However, the energy level and also the capture cross section obtained from the two samples agree fairly well.

Comparing these values with published data for Mn-related defects from the literature (see Table II for details), we are able to identify the detected impurity level with the defect level of manganese-boron pairs, which would certainly be present within the sample at the temperatures used for the DLTS measurement, namely below room temperature.

B. Injection-dependent lifetime spectroscopy (IDLS)

The effect of manganese implantation on the injection-dependent carrier lifetime is displayed in Fig. 3 for the 20 Ω cm sample. Since the lifetime of the control sample that was not implanted is about one order of magnitude higher compared to the Mn-implanted sample, it is reasonable to identify the measured lifetime of the Mn-implanted sample with the bulk lifetime. The apparent increase in lifetime below excess carrier densities of 3×10^{13} cm^{-3} is caused by measurement artifacts,[23,24] and does not reflect the true recombination lifetime. At high injection densities, Auger recombination dominates the lifetime curves, resulting in decreasing lifetime values.

In the mid-injection range, the lifetime curve has been modeled using the standard Shockley-Read-Hall (SRH)[25,26] theory for extrinsic recombination via defects. The fit (in a range from 3×10^{13} cm^{-3} to 3×10^{15} cm^{-3}) of a SRH model featuring a deep and a shallow defect center is also plotted in Fig. 3. Two separate defect centers were necessary in order to give a very good fit of the measured data.

To perform the data evaluation of the IDLS measurement with maximum transparency, the recently introduced defect parameter solution surface (DPSS)[1,17] method has been used. For the analysis of the deep defect level, the defect parameters $(E_C-E_t)_{\text{shallow}}$ and k_{shallow} ($k\equiv\sigma_n/\sigma_p$ ratio of the capture cross sections) for the additional shallow level were set to fixed values, while the SRH IDLS modeling for the deep defect level is repeated for a fixed but gradually varied defect energy depth $(E_C-E_t)_{\text{deep}}$, giving corresponding values for the k_{deep} factor and the least-squares fit error χ^2. Subsequently, the same procedure was performed for the shallow defect level with fixed values for the deep defect level. Since it was necessary to compute the fit with a shallow and a deep defect center, this routine results in two DPSS parameter sets (dashed and solid lines in Fig. 4) for the shallow and the deep defect center, respectively. Due to the inherent ambiguity of an IDLS curve at a single temperature, a corresponding k factor for any shallow and deep energy level can always be found to give a perfect fit, so only a parameter *curve* for the defect parameters can be given via analyzing the IDLS curve alone.

C. Temperature-dependent lifetime spectroscopy (TDLS)

In addition to the measurements described above, MW-PCD measurements over a temperature range from 77 to 600 K were carried out on the Mn-contaminated 20 Ω cm sample (see Fig. 5). While one TDLS curve (triangles in Fig. 5) was acquired with the sample kept in the dark in between the lifetime measurements (only very weak bias light was allowed during measurements to exclude distortions due to trapping), the other TDLS curve (circles in Fig. 5) was acquired with the sample subject to illumination with white light of approximately 0.3 W/cm^2 for at least 5 min in between two lifetime measurements at different temperatures.

The resulting graph, where the temperature normalized low-level injection lifetime is plotted against the inverse temperature (Fig. 5), exhibits three interesting temperature

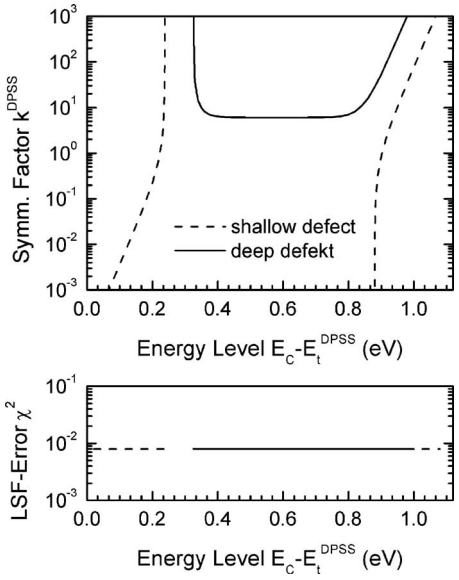

FIG. 4. DPSS analysis of the IDLS curve of the Mn-implanted 20 Ω cm sample. The errors χ^2 and ratios of the capture cross sections k of the IDLS fit for the shallow and the deep defect center are plotted for a fixed but gradually varied energy level E_C-E_t. Each parameter set for the shallow and the deep level from the diagram give the same good fit, as can be seen from the χ^2 error.

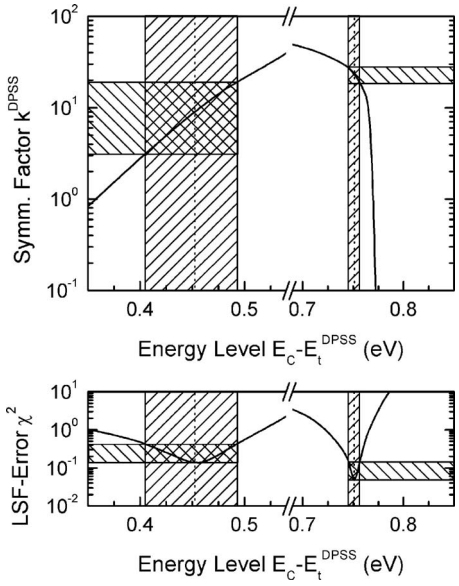

FIG. 6. DPSS analysis of the illuminated TDLS curve above a temperature of 160 °C. The error χ^2 and symmetry factor k of the TDLS are plotted for fixed but gradually varied energy level E_C-E_t. From the TDLS fit, there are two possible parameter sets possible for the Mn defect configuration above a temperature of 160 °C, one in the band gap half of the minority carriers (E_C-E_t=0.45 eV, k=9.4) and one in the band gap half of the majority carriers (E_C-E_t=0.75 eV, k=23.1).

regions. The low-level injection lifetime below a temperature of approximately −50 °C is only affected by the temperature-dependent minority carrier capture cross section. In the temperature range from −40 to +140 °C, the different lifetimes related to two different defect configurations under the two different illumination situations are clearly visible. Above a temperature of +160 °C, a linear Arrhenius increase with the onset of intrinsic conduction above +250 °C is visible.

In order to extract the defect parameters of the Mn defect configuration at higher temperatures, a TDLS fit has been performed for the illuminated curve for the high-temperature region above 160 °C using an advanced temperature model.[17] Again, the DPSS method was used for data evaluation. The TDLS fit is repeated for a fixed but gradually varied defect energy level E_C-E_t, giving corresponding values for the k factor ($=\sigma_n/\sigma_p$) and the least-squares fit error χ^2 (see Fig. 6). Two possible parameter sets with nearly the same fit quality are possible from the plot of these data triples, one in the band-gap half of the minority carriers (MinBH) (E_C-E_t=0.45 eV, k=9.4) and another in the band-gap half of the majority carriers (MajBH) (E_C-E_t=0.75 eV, k=23.1) (for details, see Table III). The uncertainties of the extracted defect parameters (shaded areas in Fig. 6) are estimated for tolerated χ^2 values of three times their optimum values. Comparing these possible data sets with reported data from the literature for Mn-related defects, we were able to relate the MinBH solution to interstitial manganese (Mn_i) (E_C-E_t=0.45 eV). The corresponding k factor can be extracted from our measurements (k=9.4) and has been determined for the first time to the best of our knowledge.

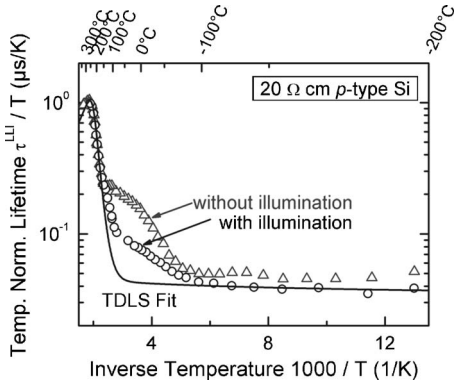

FIG. 5. Effect of light soaking and temperature on the temperature-dependent carrier lifetime under low-level injection measured by means of the MW-PCD technique on the intentionally Mn-contaminated 20 Ω cm p-type silicon sample. The lifetime was first measured without illumination (triangles) and again with illumination (I_{bias}=0.3 W/cm^2) (circles) in between the measurements. The change of defect configuration due to the illumination can be identified in a temperature range between −100 and 160 °C.

At temperatures below −70 °C, where no significant splitting of the curves due to the external illumination was observed, the modeling of the curve yielded the temperature

TABLE III. Overview of the TDLS results of the intentionally Mn-contaminated 20 Ω cm p-type silicon sample. TDLS combined with DLTS values from the literature give an unambiguous result for the defect parameters of interstitial manganese (Mn_i) in silicon located in the upper-band-gap half.

	Min BH defect		Maj BH defect	
Technique	E_C-E_t (eV)	k	E_C-E_t (eV)	k
TDLS	0.45 (0.405–0.495)	9.4 (3.2–19.0)	0.75 (0.745–0.755)	23.1 (18.5–28.3)

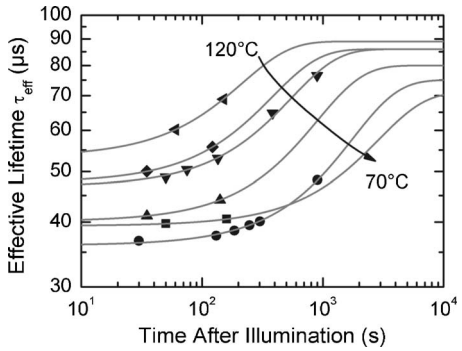

FIG. 7. Effective lifetimes measured by means of MW-PCD after the Mn-contaminated 20 Ω cm sample has been illuminated with white light (I_{bias} =0.3 W/cm^2) for at least 5 min. For every temperature, an exponential fit resulted in the (temperature-dependent) association time constant τ_{assoc}. Please note that τ_{assoc} is independent of the percentage of broken MnB pairs directly after illumination.

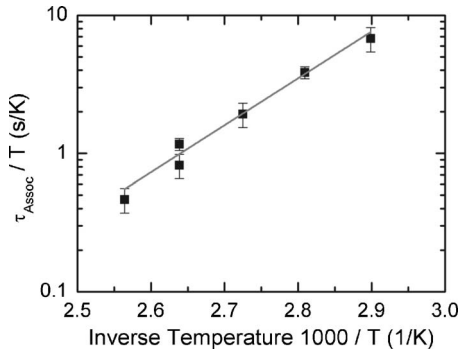

FIG. 8. Arrhenius plot of the association time constant for the intentionally Mn-contaminated 20 Ω cm sample. From the fit, the prefactor A (and hence the diffusion coefficient D_0) and the migration enthalpy H_M were determined.

dependence of the minority carrier cross section, namely $\sigma(T) \sim T^{-1.6}$, which indicates recombination via excitonic Auger capture.[27]

D. Association time constant τ_{assoc} measurement

During the TDLS measurements, it was observed that (in the temperature range between −40 and +140 °C) the lifetime values that were measured after strong illumination recovered while the sample is kept in the dark at a fixed temperature, until the lifetime value of the measurement without additional illumination is reached after some time (minutes to days, depending on the temperature). To analyze this in more detail, further measurements have been carried out for temperatures between 70 and 120 °C (see Fig. 7).

Since the measured lifetime values are a superposition of the lifetime values under illumination τ_{illum} and the lifetime values in the dark τ_{dark}, the corresponding temperature-dependent association time constant τ_{assoc} can be extracted, assuming an exponential decay and using the formula

$$\frac{1}{\tau_{measured}} = \frac{1}{\tau_{illum}} \exp\left(-\frac{t}{\tau_{assoc}}\right) + \frac{1}{\tau_{dark}} \times \left[1 - \exp\left(-\frac{t}{\tau_{assoc}}\right)\right]. \quad (1)$$

It is important to note that the fitted τ_{assoc} is correctly extracted, even if the defect configuration related to the illuminated measurement was not reached completely with the applied illumination intensity and time.

In order to analyze this Mn-related association behavior in more detail, the temperature-dependent association time constant was determined. According to Reiss *et al.*,[28] this association time constant can be calculated, assuming that the mobile ions are randomly distributed throughout the semiconductor and present in a much lower concentration than the dopant ions, as

$$\tau_{assoc} = \frac{\varepsilon \varepsilon_0 k_B T}{q^2 D N_{dop}}, \quad (2)$$

where ε is the dielectric constant of the semiconductor, ε_0 is the permittivity of free space, k_B is the Boltzmann constant, T is the absolute temperature, q is the elementary charge, D is the diffusivity of the mobile ions, and N_{dop} is the doping concentration. Using the exponential correlation for transition metals

$$D = D_0 \exp\left(-\frac{H_M}{k_B T}\right), \quad (3)$$

with D_0 signifying a temperature-independent factor and H_M the migration enthalpy, the association time constant can be rewritten as

$$\tau_{assoc} = A \frac{T}{N_{dop}} \exp\left(\frac{H_M}{k_B T}\right) \quad \text{with} \quad A = \frac{\varepsilon \varepsilon_0 k_B}{q^2 D_0}. \quad (4)$$

From the modeling of the measured τ_{assoc} values (see Fig. 8), the parameters A and H_M can be extracted as $A = 8.3 \times 10^5$ K^{-1} cm^{-3} and $H_M = 0.67$ eV from the measurements. The diffusivity coefficient D_0 can hence be calculated as $D_0 = 6.9 \times 10^{-4}$ cm^2 s^{-1}, resulting in a temperature dependence of the diffusivity as

$$D = 6.9 \times 10^{-4} \text{ cm}^2 \text{ s}^{-1} \exp\left(-\frac{0.67 \text{ eV}}{k_B T}\right). \quad (5)$$

Table IV shows a comparison of our results with reported data from the literature.[29,30] We found a nearly two-times larger diffusivity at room temperature compared to previously reported values and hence a two-times faster association of the manganese-boron pairs. The same has been recently observed for the case of interstitial iron (Fe_i) and iron-boron pairs (FeB).[31]

From the measured τ_{assoc} values, we can distinguish the observed dissociation-association behavior from Fe, since there is a factor of 3 discrepancy between the measurement results using a similar technique (see Fig. 9).

VI. CONCLUSION

Assembling the results of the defect levels of manganese in silicon for different temperatures and illumination conditions, we have identified two different defect configurations.

From the DLTS measurements, we observe that at temperatures around −50 °C, the manganese atoms are paired with boron ions and introduce a defect level within the silicon band gap at an energy of $E_t - E_V = 0.55 \pm 0.02$ eV (the

TABLE IV. Reported diffusivities for interstitial manganese in silicon. The diffusivities at 30 and 1100 °C are calculated using $D=D_0\exp(-H_M/k_BT)$. Values in brackets are calculated for a temperature region well outside the experimental temperature range.

	Diffusivity data for manganese in silicon				
Reference	T range (°C)	D_0 (cm^2/s)	H_M (eV)	D (30 °C) (cm^2/s)	D (1100 °C) (cm^2/s)
Gilles *et al.*[29]	900–1200	6.9×10^{-4}	0.63	(2.5×10^{-14})	3.4×10^{-6}
Nakashima *et al.*[30]	14–90	2.4×10^{-3}	0.72	2.8×10^{-15}	(5.5×10^{-6})
This work	70–120	6.9×10^{-4}	0.67	5.4×10^{-15}	(2.4×10^{-6})

majority carrier capture cross section is determined to be equal to $\sigma_p=3.5\times10^{-13}$ cm^2). While the experimental results exclude another defect level of MnB in the band-gap half of the majority carriers, another defect level might be possible in the band-gap half of the minority carriers.

At high temperatures (above +160 °C), all MnB pairs are dissociated so that the Mn contaminants are present in interstitial form. This result is the conclusion of TDLS measurements at high temperatures. The recombination-active defect center, which introduces interstitial Mn into the silicon band gap, is found to have the following parameters: $E_C-E_t=0.45$ eV and $k=9.4$.

The manganese-boron pairs can be broken below +160 °C (at least partially) if the sample is illuminated with strong white light (in our experiment 0.3 W/cm^2). After ceasing the illumination, the defect configuration changes as well. The (temperature-dependent) time constant of this reconfiguration process has been determined and it is shown that it differs by a factor of 3 from that for iron, determined with similar methods. It is obvious that the interstitial Mn forms MnB pairs in the intermediate range (in perfect analogy to the behavior of iron in boron-doped Si).

The interesting consequence of this implication is that a second, shallower defect level of MnB pairs might be needed. This is due to the fact that the Arrhenius increase of the MnB defect configuration is at lower temperatures compared to the Arrhenius increase of the Mn_i defect configuration (see Fig. 5), implying a shallower defect center than $E_C-E_t=0.45$ eV corresponding to the Mn_i configuration, but this has to be analyzed in more detail. Please note also that the k factor slightly influences the onset of the Arrhenius increase, but not significantly. Since the DLTS measurements

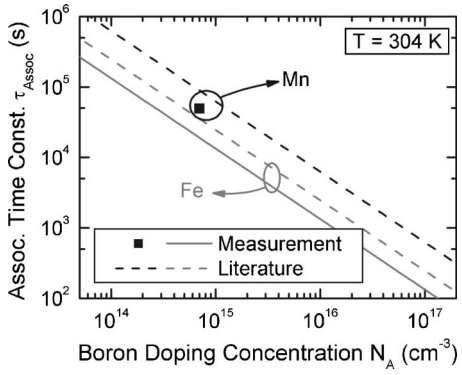

FIG. 9. Association time constant vs doping concentration determined for a temperature of $T=304$ K for iron (Ref. 31) and manganese (this work). The comparison shows the calculated values based on the diffusivity and activation energy taken from literature and the measured data.

revealed only one defect level in the band-gap half of the majority carriers, this second defect level of MnB is likely to be located within the band-gap half of the minority carriers (near the conduction band).

This implication is in good agreement with the results from the IDLS measurement, where both a deep and a shallow defect center were needed to model the measured data. Based on the DLTS measurements of the energy level ($E_t-E_V=0.55$ eV) and the majority capture cross section ($\sigma_p=3.5\times10^{-13}$ cm^2) of the deep MnB defect configuration, a minority carrier cross section of $\sigma_n=2.1\times10^{-12}$ cm^2 can be estimated in conjunction with the determined k factor of the IDLS measurement ($k=6.0$, see Fig. 4). For the possible shallow defect configuration, only the dashed line near the conduction band (see Fig. 4) can be given as a parametrization for the parameters E_t and k.

VII. SUMMARY

In this paper, a detailed study of manganese-implanted boron-doped silicon wafer by means of DLTS and lifetime spectroscopy allowed the analysis of two different defect configurations of manganese in silicon.

Concerning the defect related to manganese-boron pairs, DLTS unambiguously identified the deep defect level to be located in the lower half of the band gap at an energy level of $E_V+0.55$ eV with a majority carrier capture cross section of $\sigma_p=3.5\times10^{-13}$ cm^2. From IDLS measurements, the corresponding $k=\sigma_n/\sigma_p$ factor, which was unknown so far, could be determined to be $k=6.0$ (implying $\sigma_n=2.1\times10^{-12}$ cm^2).

Concerning the defect related to interstitial manganese, TDLS (in combination with DLTS energy level values from the literature) identified the most recombination-active defect level to be located in the upper band gap half at $E_C-0.45$ eV with a corresponding ratio of the capture cross sections of $k=9.4$. This illustrates the ability of lifetime spectroscopy to identify the most dominant recombination level.

From dynamic TDLS measurements, the temperature-dependent association time constant of the formation of manganese-boron pairs could be determined and can be represented by the expression $\tau_{assoc}=8.3\times10^5$ K^{-1} cm^{-3} $(T/N_{dop})\exp(0.67\ \text{eV}/k_BT)$. From these measurements, the diffusivity coefficient D_0 and the migration enthalpy H_M have been determined (in a temperature range from 70 to 120 °C) to be $D_0=6.9\times10^{-4}$ cm^2 s^{-1} and $H_M=0.67$ eV. Compared with literature values for the diffusivity, this is two times faster than expected, but is consistent with recent findings regarding iron-boron pairs using similar experimental techniques.

The association time constant for MnB pairs was found to be three times slower than for iron-boron pairs. This may be used as a fingerprint to identify possible contamination with manganese.

ACKNOWLEDGMENTS

One of the authors (T.R.) gratefully acknowledges a scholarship of the German Federal Environmental Foundation (Deutsche Bundesstiftung Umwelt). Another (D.M.) is supported by an Australian Research Council QEII Fellowship. The authors are also grateful to J. Holtkamp and S. Rein of Fraunhofer ISE for their support and fruitful discussions, and to R. Elliman, C. Jagadish, and H. Tan of ANU for access to the ion implantation and PECVD equipment.

[1]S. Rein and S. W. Glunz, Appl. Phys. Lett. **82**, 1054 (2003).
[2]K. Graff, *Metal Impurities in Silicon-Device Fabrication*, 2nd ed. (Springer, Berlin, 1999), Vol. 24.
[3]G. W. Ludwig and H. H. Woodbury, Phys. Rev. Lett. **5**, 98 (1960).
[4]G. W. Ludwig and H. H. Woodbury, Solid State Phys. **13**, 223 (1962).
[5]R. O. Carlson, Phys. Rev. **104**, 937 (1956).
[6]H. Nakashima and K. Hashimoto, J. Appl. Phys. **69**, 1440 (1991).
[7]H. Lemke, Phys. Status Solidi A **64**, 549 (1981).
[8]H. Lemke, Phys. Status Solidi A **72**, 177 (1982).
[9]M. Haider, H. Sitter, R. Czaputa, H. Feichtinger, and J. Oswald, J. Appl. Phys. **62**, 3785 (1987).
[10]H. Lemke, Phys. Status Solidi A **83**, 637 (1984).
[11]R. Czaputa, H. Feichtinger, J. Oswald, H. Sitter, and M. Haider, Phys. Rev. Lett. **55**, 758 (1985).
[12]D. Macdonald, P. N. K. Deenapanray, and S. Diez, J. Appl. Phys. **96**, 3687 (2004).
[13]D. Gilles, W. Schröter, and W. Bergholz, Phys. Rev. B **41**, 5770 (1990).
[14]P. Rosenits and D. Macdonald, Proceedings of the 21st European Photovoltaic Solar Energy Conference, Dresden, Germany (WIP, Munich, 2006), pp. 953–956.
[15]D. Macdonald, P. Rosenits, and P. N. K. Deenapanray, Semicond. Sci. Technol. **22**, 163 (2007).
[16]D. V. Lang, J. Appl. Phys. **45**, 3023 (1974).
[17]S. Rein, *Lifetime Spectroscopy: A Method of Defect Characterization in Silicon for Photovoltaic Applications* (Springer, Berlin, 2005).
[18]R. A. Sinton, A. Cuevas, and M. Stuckings, *Proceedings of the 25th IEEE Photovoltaic Specialists Conference*, Washington DC (1996), pp. 457–460.
[19]U. Creutzburg, PhD thesis, Universität Bremen (1991).
[20]M. Schöfthaler and R. Brendel, J. Appl. Phys. **77**, 3162 (1995).
[21]S. W. Glunz, J. Schumacher, W. Warta, J. Knobloch, and W. Wettling, Prog. Photovoltaics **4**, 415 (1996).
[22]A. A. Istratov, H. Hieslmair, and E. R. Weber, Appl. Phys. A: Mater. Sci. Process. **69**, 13 (1999).
[23]D. Macdonald and A. Cuevas, Appl. Phys. Lett. **74**, 1710 (1999).
[24]P. J. Cousins, D. H. Neuhaus, and J. E. Cotter, J. Appl. Phys. **95**, 1854 (2004).
[25]W. Shockley and W. T. J. Read, Phys. Rev. **87**, 835 (1952).
[26]R. N. Hall, Phys. Rev. **87**, 387 (1952).
[27]A. Hangleiter, Phys. Rev. B **35**, 9149 (1987).
[28]H. Reiss, C. S. Fuller, and F. J. Morin, Bell Syst. Tech. J. **35**, 535 (1956).
[29]D. Gilles, W. Bergholz, and W. Schröter, J. Appl. Phys. **59**, 3590 (1986).
[30]H. Nakashima, T. Sadoh, H. Kitagawa, and K. Hashimoto, Proceedings of the 17th International Conference on Defects in Semiconductors (Trans. Tech. Publications, Switzerland, 1993), pp. 761–766.
[31]D. Macdonald, T. Roth, P. N. K. Deenapanray, K. Bothe, P. Pohl, and J. Schmidt, J. Appl. Phys. **98**, 083509 (2005).